

The ground state energy at unitarity

Dean Lee

Department of Physics, North Carolina State University, Raleigh, NC 27695

Abstract

We consider two-component fermions on the lattice in the unitarity limit. This is an idealized limit of attractive fermions where the range of the interaction is zero and the scattering length is infinite. Using Euclidean time projection, we compute the ground state energy using four computationally different but physically identical auxiliary-field methods. The best performance is obtained using a bounded continuous auxiliary field and a non-local updating algorithm called hybrid Monte Carlo. With this method we calculate results for 10 and 14 fermions at lattice volumes $4^3, 5^3, 6^3, 7^3, 8^3$ and extrapolate to the continuum limit. For 10 fermions in a periodic cube, the ground state energy is 0.292(12) times the ground state energy for non-interacting fermions. For 14 fermions the ratio is 0.329(5).

I. INTRODUCTION

The unitarity limit describes attractive two-component fermions in an idealized limit where the range of the interaction is zero and the scattering length is infinite. The name refers to the fact that the S-wave cross section saturates the limit imposed by unitarity, $\sigma_0(k) \leq 4\pi/k^2$, for low momenta k . In the unitarity limit details about the microscopic interaction are lost, and the system displays universal properties. Throughout our discussion we refer to the two degenerate components as up and down spins, though the correspondence with actual spin is not necessary. At sufficiently low temperatures the spin-unpolarized system is believed to be superfluid with properties in between a Bardeen-Cooper-Schrieffer (BCS) fermionic superfluid at weak coupling and a Bose-Einstein condensate of dimers at strong coupling [1, 2, 3].

In nuclear physics the phenomenology of the unitarity limit is relevant to cold dilute neutron matter. The scattering length for elastic neutron-neutron collisions is about -18.5 fm while the range of the interaction is comparable to the Compton wavelength of the pion, $m_\pi^{-1} \approx 1.4$ fm. Therefore the unitarity limit is approximately realized when the interparticle spacing is about 5 fm. While these conditions cannot be produced experimentally, neutrons at around this density may be present in the inner crust of neutron stars [4, 5].

The unitarity limit has been experimentally realized with cold atomic Fermi gases. For alkali atoms the relevant length scale for the interatomic potential at long distances is the van der Waals length ℓ_{vdW} . If the spacing between atoms is much larger than ℓ_{vdW} , then to a good approximation the interatomic potential is equivalent to a zero range interaction. The scattering length can be manipulated using a magnetic Feshbach resonance [6, 7, 8, 9, 10, 11, 12]. This technique involves a molecular bound state in a “closed” hyperfine channel crossing the scattering threshold of an “open” channel. The magnetic moments for the two channels are typically different, and so the crossing can be produced using an applied magnetic field.

At zero temperature there are no dimensionful parameters other than particle density. For N_\uparrow up spins and N_\downarrow down spins in a given volume we write the energy of the unitarity-limit ground state as $E_{N_\uparrow, N_\downarrow}^0$. For the same volume we call the energy of the free non-interacting ground state $E_{N_\uparrow, N_\downarrow}^{0, \text{free}}$, and the dimensionless ratio of the two $\xi_{N_\uparrow, N_\downarrow}$,

$$\xi_{N_\uparrow, N_\downarrow} = E_{N_\uparrow, N_\downarrow}^0 / E_{N_\uparrow, N_\downarrow}^{0, \text{free}}. \quad (1)$$

The parameter ξ is defined as the thermodynamic limit for the spin-unpolarized system,

$$\xi = \lim_{N \rightarrow \infty} \xi_{N,N}. \quad (2)$$

Several experiments have measured ξ from the expansion of ${}^6\text{Li}$ and ${}^{40}\text{K}$ released from a harmonic trap. Some recent measured values for ξ are 0.51(4) [12], $0.46_{-0.05}^{+0.12}$ [13], and $0.32_{-0.13}^{+0.10}$ [11]. The disagreement between these measurements and larger values for ξ reported in earlier experiments [6, 9, 10] suggest further work may be needed.

There are numerous analytic calculations of ξ using a variety of techniques such as BCS saddle point and variational approximations, Padé approximations, mean field theory, density functional theory, exact renormalization group, dimensional ϵ -expansions, and large- N expansions [14, 15, 16, 17, 18, 19, 20, 21, 22, 23, 24, 25, 26]. The values for ξ range from 0.2 to 0.6. Fixed-node Green's function Monte Carlo simulations for a periodic cube have found $\xi_{N,N}$ to be 0.44(1) for $5 \leq N \leq 21$ [27] and 0.42(1) for larger N [28, 29]. A restricted path integral Monte Carlo calculation finds similar results [30], and a sign-restricted mean field lattice calculation yields 0.449(9) [31].

There have also been simulations of two-component fermions on the lattice in the unitarity limit at nonzero temperature. When data are extrapolated to zero temperature the results of [32, 33] produce a value for ξ similar to the fixed-node results. The same is true for [34, 35], though with significant error bars. The extrapolated zero temperature lattice results from [36, 37] established a bound, $0.07 \leq \xi \leq 0.42$, while more recent lattice calculations yield 0.261(12) [38, 39]. The work of [38, 39] includes a comparison of two lattice algorithms similar to the ones discussed in this paper.

In [40] $\xi_{N,N}$ was calculated on the lattice using Euclidean time projection for $N = 3, 5, 7, 9, 11$ and lattice volumes $4^3, 5^3, 6^3$. From these small volumes it was estimated that $\xi = 0.25(3)$. More recent results using a technique called the symmetric heavy-light ansatz found similar values for $\xi_{N,N}$ at the same lattice volumes and estimated $\xi = 0.31(1)$ in the continuum and thermodynamic limits [41].

For lattice calculations of $\xi_{N,N}$ at fixed N , systematic errors due to nonzero lattice spacing can be removed by extrapolating to the continuum limit. At unitarity where the scattering length is set to infinity, this continuum extrapolation corresponds with increasing the lattice volume as measured in lattice units. In this paper we present new lattice results using the Euclidean time projection method introduced in [40] and extrapolate to the continuum

limit.

In earlier work [40, 42] singular matrices were encountered that prevented calculations at larger volumes. We discuss this and related issues by considering four different auxiliary-field methods which reproduce exactly the same Euclidean lattice model. These four methods include a Gaussian-integral auxiliary field, an exponentially-coupled auxiliary field, a discrete auxiliary field, and a bounded continuous auxiliary field. By far the best performance is obtained using the bounded continuous auxiliary field and hybrid Monte Carlo [43]. With this method we calculate the ground state energy for 10 and 14 fermions at lattice volumes $4^3, 5^3, 6^3, 7^3, 8^3$ and extrapolate to the continuum limit.

II. EUCLIDEAN TIME LATTICE FORMALISM

Throughout our discussion of the lattice formalism we use dimensionless parameters and operators corresponding with physical values multiplied by the appropriate power of the spatial lattice spacing a . In our notation the three-component integer vector \vec{n} labels the lattice sites of a three-dimensional periodic lattice with dimensions L^3 . The spatial lattice unit vectors are denoted $\hat{l} = \hat{1}, \hat{2}, \hat{3}$. We use n_t to label lattice steps in the temporal direction. L_t denotes the total number of lattice time steps. The temporal lattice spacing is given by a_t , and $\alpha_t = a_t/a$ is the ratio of the temporal to spatial lattice spacing. We also define $h = \alpha_t/(2m)$, where m is the fermion mass in lattice units.

We discuss four different formulations of the Euclidean time lattice for interacting fermions: Grassmann path integrals with and without auxiliary field and transfer matrix operators with and without auxiliary field. For any spatial and temporal lattice spacings these four formulations produce exactly the same physics, as indicated in Fig. 1. We follow the order of discussion indicated by the numbered arrows in Fig. 1.

A. Grassmann path integral without auxiliary field

Let c_i and c_i^* be anticommuting Grassmann fields for spin i . The Grassmann fields are periodic with respect to the spatial lengths of the L^3 lattice,

$$c_i(\vec{n} + L\hat{1}, n_t) = c_i(\vec{n} + L\hat{2}, n_t) = c_i(\vec{n} + L\hat{3}, n_t) = c_i(\vec{n}, n_t), \quad (3)$$

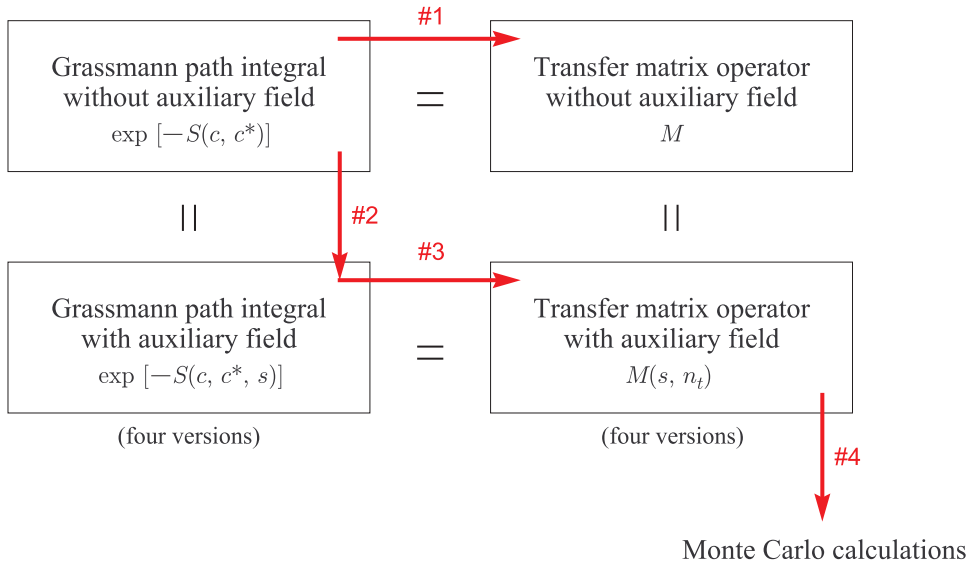


FIG. 1: (Color online) Schematic diagram showing four equivalent Euclidean time lattice formulations. The numbered arrows indicate the order of discussion in the text.

and antiperiodic along the temporal direction,

$$c_i(\vec{n}, n_t + L_t) = -c_i(\vec{n}, n_t). \quad (4)$$

We write $DcDc^*$ as shorthand for the integral measure,

$$DcDc^* = \prod_{\vec{n}, n_t, i=\uparrow, \downarrow} dc_i(\vec{n}, n_t) dc_i^*(\vec{n}, n_t). \quad (5)$$

The Grassmann spin densities, ρ_\uparrow and ρ_\downarrow , are defined as

$$\rho_\uparrow(\vec{n}, n_t) = c_\uparrow^*(\vec{n}, n_t) c_\uparrow(\vec{n}, n_t), \quad (6)$$

$$\rho_\downarrow(\vec{n}, n_t) = c_\downarrow^*(\vec{n}, n_t) c_\downarrow(\vec{n}, n_t). \quad (7)$$

We consider the Grassmann path integral

$$\mathcal{Z} = \int DcDc^* \exp[-S(c, c^*)], \quad (8)$$

$$S(c, c^*) = S_{\text{free}}(c, c^*) + C\alpha_t \sum_{\vec{n}, n_t} \rho_\uparrow(\vec{n}, n_t) \rho_\downarrow(\vec{n}, n_t). \quad (9)$$

The action $S(c, c^*)$ consists of the free fermion action

$$\begin{aligned}
S_{\text{free}}(c, c^*) = & \sum_{\vec{n}, n_t, i=\uparrow, \downarrow} [c_i^*(\vec{n}, n_t) c_i(\vec{n}, n_t + 1) - (1 - 6h) c_i^*(\vec{n}, n_t) c_i(\vec{n}, n_t)] \\
& - h \sum_{\vec{n}, n_t, i=\uparrow, \downarrow} \sum_{l=1,2,3} \left[c_i^*(\vec{n}, n_t) c_i(\vec{n} + \hat{l}, n_t) + c_i^*(\vec{n}, n_t) c_i(\vec{n} - \hat{l}, n_t) \right], \quad (10)
\end{aligned}$$

and an attractive contact interaction between up and down spins. We take this action as the definition of the lattice model. All other formulations introduced later will be shown to be exactly equivalent.

We use a fermion mass of 939 MeV and lattice spacings $a = (50 \text{ MeV})^{-1}$, $a_t = (24 \text{ MeV})^{-1}$. In dimensionless lattice units the corresponding parameters are $m = 18.78$ and $\alpha_t = 2.0833$. These are the same values used in [40] and is motivated by the relevant physical scales for dilute neutron matter.

B. Interaction coefficient C for general spatial and temporal lattice spacings

We use Lüscher's formula [44, 45, 46, 47] to relate the coefficient C to the S-wave scattering length. We consider one up-spin particle and one down-spin particle in a periodic cube of length L . Lüscher's formula relates the two-particle energy levels in the center-of-mass frame to the S-wave phase shift,

$$p \cot \delta_0(p) = \frac{1}{\pi L} S(\eta), \quad \eta = \left(\frac{Lp}{2\pi} \right)^2, \quad (11)$$

where $S(\eta)$ is the three-dimensional zeta function,

$$S(\eta) = \lim_{\Lambda \rightarrow \infty} \left[\sum_{\vec{n}} \frac{\theta(\Lambda^2 - \vec{n}^2)}{\vec{n}^2 - \eta} - 4\pi\Lambda \right]. \quad (12)$$

For small momenta the effective range expansion gives

$$p \cot \delta_0(p) \approx -\frac{1}{a_{\text{scatt}}} + \frac{1}{2} r_0 p^2 + \dots, \quad (13)$$

where a_{scatt} is the scattering length and r_0 is the effective range.

In terms of η , the energy of the two-particle scattering state is

$$E_{\text{pole}} = \frac{p^2}{m} = \frac{\eta}{m} \left(\frac{2\pi}{L} \right)^2. \quad (14)$$

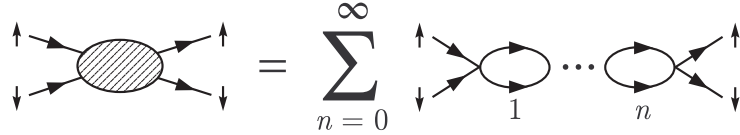


FIG. 2: Sum of bubble diagrams contributing to two-particle scattering.

We compute the location of the two-particle scattering pole by summing the bubble diagrams shown in Fig. 2. After writing the sum of bubble diagrams as a geometric series, the relation between C and E_{pole} becomes

$$-\frac{1}{C\alpha_t} = \lim_{L \rightarrow \infty} \frac{1}{L^3} \sum_{\vec{k} \text{ integer}} \frac{1}{e^{-E_{\text{pole}}\alpha_t} - 1 + 2\alpha_t\omega(2\pi\vec{k}/L) - \alpha_t^2\omega^2(2\pi\vec{k}/L)}, \quad (15)$$

where

$$\omega(\vec{p}) = \frac{1}{m} \sum_{l=1,2,3} (1 - \cos p_l). \quad (16)$$

These expressions were first derived in [48]. In the unitarity limit the scattering length a_{scatt} is set to infinity and all other effective range parameters are set to zero. From Eq. (13) and (11) this is equivalent to setting $S(\eta) = 0$. To minimize lattice discretization errors we pick the root of $S(\eta)$ closest to zero, $\eta = -0.095901$. After selecting some large value for L , we use Eq. (14) and (15) to determine the unitarity limit value for the coefficient C . For our chosen lattice parameters C is -7.4415×10^{-5} MeV $^{-2}$ in physical units or -0.18604 in dimensionless lattice units.

C. Transfer matrix operator without auxiliary field

We convert the Grassmann path integral into the trace of a product of transfer matrix operators using the exact correspondence [49, 50]

$$\begin{aligned} & Tr \left\{ : F_{L_t-1} [a_{i'}^\dagger(\vec{n}'), a_i(\vec{n})] : \cdots : F_0 [a_{i'}^\dagger(\vec{n}'), a_i(\vec{n})] : \right\} \\ &= \int DcDc^* \exp \left\{ \sum_{n_t=0}^{L_t-1} \sum_{\vec{n}, i} c_i^*(\vec{n}, n_t) [c_i(\vec{n}, n_t) - c_i(\vec{n}, n_t + 1)] \right\} \\ & \quad \times \prod_{n_t=0}^{L_t-1} F_{n_t} [c_{i'}^*(\vec{n}', n_t), c_i(\vec{n}, n_t)], \end{aligned} \quad (17)$$

where $c_i(\vec{n}, L_t) = -c_i(\vec{n}, 0)$. We use $a_i(\vec{n})$ and $a_i^\dagger(\vec{n})$ to denote fermion annihilation and creation operators respectively for spin i at lattice site \vec{n} . The $:$ symbols in (17) indicate normal ordering. Let us define

$$H_{\text{free}} = \frac{3}{m} \sum_{\vec{n}, i=\uparrow, \downarrow} a_i^\dagger(\vec{n}) a_i(\vec{n}) - \frac{1}{2m} \sum_{\vec{n}, i=\uparrow, \downarrow} \sum_{l=1,2,3} \left[a_i^\dagger(\vec{n}) a_i(\vec{n} + \hat{l}) + a_i^\dagger(\vec{n}) a_i(\vec{n} - \hat{l}) \right] \quad (18)$$

and

$$\rho_\uparrow^{a^\dagger a}(\vec{n}) = a_\uparrow^\dagger(\vec{n}) a_\uparrow(\vec{n}), \quad (19)$$

$$\rho_\downarrow^{a^\dagger a}(\vec{n}) = a_\downarrow^\dagger(\vec{n}) a_\downarrow(\vec{n}). \quad (20)$$

Then

$$\mathcal{Z} = \text{Tr} (M^{L_t}), \quad (21)$$

where M is the normal-ordered transfer matrix operator

$$M =: \exp \left[-H_{\text{free}} \alpha_t - C \alpha_t \sum_{\vec{n}} \rho_\uparrow^{a^\dagger a}(\vec{n}) \rho_\downarrow^{a^\dagger a}(\vec{n}) \right] :. \quad (22)$$

D. Grassmann path integral with auxiliary field

We consider four different auxiliary-field transformations labelled with the subscript $j = 1, 2, 3, 4$. Let us define the Grassmann actions

$$S_j(c, c^*, s) = S_{\text{free}}(c, c^*) - \sum_{\vec{n}, n_t} A_j [s(\vec{n}, n_t)] \cdot [\rho_\uparrow(\vec{n}, n_t) + \rho_\downarrow(\vec{n}, n_t)], \quad (23)$$

and Grassmann path integrals

$$\mathcal{Z}_j = \prod_{\vec{n}, n_t} \left[\int d_j s(\vec{n}, n_t) \right] \int Dc Dc^* \exp [-S_j(c, c^*, s)], \quad (24)$$

where s is a real-valued function over all lattice sites. For $j = 1$, we use a Gaussian-integral transformation similar to the original Hubbard-Stratonovich transformation [51, 52],

$$\int d_1 s(\vec{n}, n_t) = \frac{1}{\sqrt{2\pi}} \int_{-\infty}^{+\infty} ds(\vec{n}, n_t) e^{-\frac{1}{2} s^2(\vec{n}, n_t)}, \quad (25)$$

$$A_1 [s(\vec{n}, n_t)] = \sqrt{-C_1 \alpha_t} s(\vec{n}, n_t). \quad (26)$$

For $j = 2$ we use an auxiliary field with exponential coupling to the fermion densities,

$$\int d_2 s(\vec{n}, n_t) = \frac{1}{\sqrt{2\pi}} \int_{-\infty}^{+\infty} ds(\vec{n}, n_t) e^{-\frac{1}{2} s^2(\vec{n}, n_t)}, \quad (27)$$

$$A_2 [s(\vec{n}, n_t)] = (1 - 6h) \left[e^{\sqrt{-C_2\alpha_t} s(\vec{n}, n_t) + \frac{C_2\alpha_t}{2}} - 1 \right]. \quad (28)$$

This is the auxiliary-field transformation used in [36, 37, 40, 42, 48]. For $j = 3$ we use a discrete auxiliary field taking values -1 or $+1$ at each lattice site,

$$\int d_3 s(\vec{n}, n_t) = \frac{1}{2} \sum_{s(\vec{n}, n_t) = \pm 1}, \quad (29)$$

$$A_3 [s(\vec{n}, n_t)] = \sqrt{-C_3\alpha_t} s(\vec{n}, n_t). \quad (30)$$

The discrete Hubbard-Stratonovich transformation was first introduced by Hirsch in [53] and has been used in a number of recent lattice simulations [32, 33, 38, 39, 54]. For $j = 4$ we introduce a new transformation which uses a bounded but continuous auxiliary field,

$$\int d_4 s(\vec{n}, n_t) = \frac{1}{2\pi} \int_{-\pi}^{+\pi} ds(\vec{n}, n_t), \quad (31)$$

$$A_4 [s(\vec{n}, n_t)] = \sqrt{-C_4\alpha_t} \sin [s(\vec{n}, n_t)]. \quad (32)$$

The motivation for the new transformation is discussed later when comparing and analyzing computational performance.

For each $j = 1, 2, 3, 4$ the integral transformations are defined so that

$$\int d_j s(\vec{n}, n_t) 1 = 1, \quad (33)$$

$$\int d_j s(\vec{n}, n_t) A_j [s(\vec{n}, n_t)] = 0. \quad (34)$$

Since all even products of Grassmann variables commute, we can factor out the term in \mathcal{Z}_j involving the auxiliary field s at \vec{n}, n_t . To shorten the notation we temporarily omit writing \vec{n}, n_t explicitly. For each $j = 1, 2, 3, 4$ we find

$$\begin{aligned} \int d_j s \exp [A_j (s) (\rho_\uparrow + \rho_\downarrow)] &= \int d_j s [1 + A_j (s) (\rho_\uparrow + \rho_\downarrow) + A_j^2 (s) \rho_\uparrow \rho_\downarrow] \\ &= 1 + \int d_j s A_j^2 (s) \rho_\uparrow \rho_\downarrow = \exp \left[\int d_j s A_j^2 (s) \rho_\uparrow \rho_\downarrow \right]. \end{aligned} \quad (35)$$

For the four cases the integral of A_j^2 is

$$\int d_1 s A_1^2 (s) = -C_1\alpha_t, \quad (36)$$

$$\int d_2 s A_2^2 (s) = (1 - 6h)^2 (e^{-C_2\alpha_t} - 1), \quad (37)$$

TABLE I: Filling sequence of momentum states for each spin.

N	additional momenta filled
1	$\langle 0, 0, 0 \rangle$
3	$\langle \frac{2\pi}{L}, 0, 0 \rangle, \langle -\frac{2\pi}{L}, 0, 0 \rangle$
5	$\langle 0, \frac{2\pi}{L}, 0 \rangle, \langle 0, -\frac{2\pi}{L}, 0 \rangle$
7	$\langle 0, 0, \frac{2\pi}{L} \rangle, \langle 0, 0, -\frac{2\pi}{L} \rangle$

$$\int d_3s A_3^2(s) = -C_3\alpha_t, \quad (38)$$

$$\int d_4s A_4^2(s) = -\frac{1}{2}C_4\alpha_t. \quad (39)$$

Therefore

$$\mathcal{Z} = \mathcal{Z}_1 = \mathcal{Z}_2 = \mathcal{Z}_3 = \mathcal{Z}_4 \quad (40)$$

when the interaction coefficients satisfy

$$C = C_1 = -\frac{(1-6h)^2(e^{-C_2\alpha_t} - 1)}{\alpha_t} = C_3 = \frac{1}{2}C_4. \quad (41)$$

III. TRANSFER MATRIX OPERATOR WITH AUXILIARY FIELD

Using Eq. (17) and (40) we can write \mathcal{Z} as a product of transfer matrix operators which depend on the auxiliary fields,

$$\mathcal{Z} = \prod_{\vec{n}, n_t} \left[\int d_j s(\vec{n}, n_t) \right] Tr \{ M_j(s, L_t - 1) \cdots M_j(s, 0) \}, \quad (42)$$

where

$$M_j(s, n_t) =: \exp \left\{ -H_{\text{free}}\alpha_t + \sum_{\vec{n}} A_j[s(\vec{n}, n_t)] \cdot \left[\rho_{\uparrow}^{a\dagger}(\vec{n}) + \rho_{\downarrow}^{a\dagger}(\vec{n}) \right] \right\} :. \quad (43)$$

For the numerical lattice calculations presented in this paper we use the auxiliary-field transfer matrix operators in Eq. (43).

Let $|\Psi_{N,N}^{0,\text{free}}\rangle$ be the normalized Slater-determinant ground state on the lattice for a non-interacting system of N up spins and N down spins. For each spin we fill momentum states in the order shown in Table I. We construct the Euclidean time projection amplitude

$$Z_{N,N}(t) \equiv \prod_{\vec{n}, n_t} \left[\int d_j s(\vec{n}, n_t) \right] \langle \Psi_{N,N}^{0,\text{free}} | M_j(s, L_t - 1) \cdots M_j(s, 0) | \Psi_{N,N}^{0,\text{free}} \rangle, \quad (44)$$

where $t = L_t \alpha_t$. The result upon integration gives the same $Z_{N,N}(t)$ for each $j = 1, 2, 3, 4$.

As a result of normal ordering, $M_j(s, n_t)$ consists of only single-particle operators interacting with the background auxiliary field and no direct interactions between particles. We find

$$\left\langle \Psi_{N,N}^{0,\text{free}} \left| M_j(s, L_t - 1) \cdots M_j(s, 0) \right| \Psi_{N,N}^{0,\text{free}} \right\rangle = [\det \mathbf{M}_j(s, t)]^2, \quad (45)$$

where

$$[\mathbf{M}_j(s, t)]_{k'k} = \langle \vec{p}_{k'} | M_j(s, L_t - 1) \cdots M_j(s, 0) | \vec{p}_k \rangle, \quad (46)$$

for matrix indices $k, k' = 1, \dots, N$. $|\vec{p}_k\rangle, |\vec{p}_{k'}\rangle$ are single-particle momentum states comprising the Slater-determinant initial/final state. The single-particle interactions in $M_j(s, n_t)$ are the same for both up and down spins, and this is why the determinant in Eq. (45) is squared. Since the matrix is real-valued, the square of the determinant is nonnegative and there is no problem with oscillating signs.

For the interacting lattice system at unitarity, we label the energy eigenstates $|\Psi_{N,N}^k\rangle$ with energies $E_{N,N}^k$ in order of increasing energy,

$$E_{N,N}^0 \leq E_{N,N}^1 \leq \cdots \leq E_{N,N}^k \leq \cdots \quad (47)$$

In the transfer matrix formalism these energies are defined in terms of the logarithm of the transfer matrix eigenvalue,

$$M |\Psi_{N,N}^k\rangle = e^{-E_{N,N}^k \alpha_t} |\Psi_{N,N}^k\rangle. \quad (48)$$

Let us define $c_{N,N}^k$ as the inner product with the initial free fermion ground state,

$$c_{N,N}^k = \langle \Psi_{N,N}^k | \Psi_{N,N}^{0,\text{free}} \rangle. \quad (49)$$

In the following we assume that $c_{N,N}^0$, the overlap between free fermion ground state and the interacting ground state, is nonzero.

Let us define a transient energy expectation value that depends on the Euclidean time t ,

$$E_{N,N}(t) = \frac{1}{\alpha_t} \ln \frac{Z_{N,N}(t - \alpha_t)}{Z_{N,N}(t)}. \quad (50)$$

The spectral decomposition of $Z_{N,N}(t)$ gives

$$Z_{N,N}(t) = \sum_k |c_{N,N}^k|^2 e^{-E_{N,N}^k t}, \quad (51)$$

and at large Euclidean time t significant contributions come from only low energy eigenstates. For large t we find

$$E_{N,N}(t) \approx E_{N,N}^0 + \sum_{k \neq 0} \frac{|c_{N,N}^k|^2}{|c_{N,N}^0|^2} \frac{e^{(E_{N,N}^k - E_{N,N}^0)\alpha_t} - 1}{\alpha_t} e^{-(E_{N,N}^k - E_{N,N}^0)t}. \quad (52)$$

For low energy excitations $E_{N,N}^k - E_{N,N}^0$ is much smaller than the energy cutoff scale α_t^{-1} imposed by the temporal lattice spacing. Therefore

$$E_{N,N}(t) \approx E_{N,N}^0 + \sum_{k \neq 0} \frac{|c_{N,N}^k|^2}{|c_{N,N}^0|^2} (E_{N,N}^k - E_{N,N}^0) e^{-(E_{N,N}^k - E_{N,N}^0)t}. \quad (53)$$

The ground state energy $E_{N,N}^0$ is given by the limit

$$E_{N,N}^0 = \lim_{t \rightarrow \infty} E_{N,N}(t). \quad (54)$$

IV. IMPORTANCE SAMPLING

We calculate the ratio

$$\frac{Z_{N,N}(t - \alpha_t)}{Z_{N,N}(t)} \quad (55)$$

using Markov chain Monte Carlo. For $t = L_t \alpha_t$, configurations for the auxiliary field are sampled according to the weight

$$\exp \{-U_j(s) + 2 \ln [|\det \mathbf{M}_j(s, L_t \alpha_t)|]\}, \quad (56)$$

where

$$U_1(s) = U_2(s) = \frac{1}{2} \sum_{\vec{n}, n_t} [s(\vec{n}, n_t)]^2, \quad (57)$$

and

$$U_3(s) = U_4(s) = 0. \quad (58)$$

For $j = 1, 2, 4$ importance sampling is implemented using hybrid Monte Carlo [43]. This involves computing molecular dynamics trajectories for

$$H_j(s, p) = \frac{1}{2} \sum_{\vec{n}, n_t} [p(\vec{n}, n_t)]^2 + V_j(s), \quad (59)$$

where $p(\vec{n}, n_t)$ is the conjugate momentum for $s(\vec{n}, n_t)$ and

$$V_j(s) = U_j(s) - 2 \ln [|\det \mathbf{M}_j(s, L_t \alpha_t)|]. \quad (60)$$

The steps of the algorithm are as follows.

Step 1: Select an arbitrary initial configuration s^0 .

Step 2: Select a configuration p^0 according to the Gaussian random distribution

$$P [p^0(\vec{n}, n_t)] \propto \exp \left\{ -\frac{1}{2} [p^0(\vec{n}, n_t)]^2 \right\}. \quad (61)$$

Step 3: For each \vec{n}, n_t let

$$\tilde{p}^0(\vec{n}, n_t) = p^0(\vec{n}, n_t) - \frac{\varepsilon_{\text{step}}}{2} \left[\frac{\partial V_j(s)}{\partial s(\vec{n}, n_t)} \right]_{s=s^0} \quad (62)$$

for some small positive $\varepsilon_{\text{step}}$. The derivative of V_j is computed using

$$\begin{aligned} \frac{\partial V_j(s)}{\partial s(\vec{n}, n_t)} &= \frac{\partial U_j(s)}{\partial s(\vec{n}, n_t)} - \frac{2}{\det \mathbf{M}_j} \sum_{k,l} \frac{\partial \det \mathbf{M}_j}{\partial [\mathbf{M}_j]_{kl}} \frac{\partial [\mathbf{M}_j]_{kl}}{\partial s(\vec{n}, n_t)} \\ &= \frac{\partial U_j(s)}{\partial s(\vec{n}, n_t)} - 2 \sum_{k,l} [\mathbf{M}_j^{-1}]_{lk} \frac{\partial [\mathbf{M}_j]_{kl}}{\partial s(\vec{n}, n_t)}. \end{aligned} \quad (63)$$

Step 4: For steps $i = 0, 1, \dots, N_{\text{step}} - 1$, let

$$s^{i+1}(\vec{n}, n_t) = s^i(\vec{n}, n_t) + \varepsilon_{\text{step}} \tilde{p}^i(\vec{n}, n_t), \quad (64)$$

$$\tilde{p}^{i+1}(\vec{n}, n_t) = \tilde{p}^i(\vec{n}, n_t) - \varepsilon_{\text{step}} \left[\frac{\partial V_j(s)}{\partial s(\vec{n}, n_t)} \right]_{s=s^{i+1}}, \quad (65)$$

for each \vec{n}, n_t .

Step 5: For each \vec{n}, n_t let

$$p^{N_{\text{step}}}(\vec{n}, n_t) = \tilde{p}^{N_{\text{step}}}(\vec{n}, n_t) + \frac{\varepsilon_{\text{step}}}{2} \left[\frac{\partial V(s)}{\partial s(\vec{n}, n_t)} \right]_{s=s^{N_{\text{step}}}}. \quad (66)$$

Step 6: Select a random number $r \in [0, 1)$. If

$$r < \exp [-H(s^{N_{\text{step}}}, p^{N_{\text{step}}}) + H(s^0, p^0)] \quad (67)$$

then set $s^0 = s^{N_{\text{step}}}$. Otherwise leave s^0 as is. In either case go back to Step 2 to start a new trajectory.

For $j = 3$, hybrid Monte Carlo cannot be used since the auxiliary field has only discrete values -1 or $+1$. In this case we use a local Metropolis accept/reject update. For each sweep through the entire lattice a small fraction of random lattice sites are selected. A new configuration s' is produced by flipping the sign of s at these sites. A random number $r \in$

$[0, 1)$ is selected and the new configuration s' is accepted or rejected based on the Metropolis condition,

$$r < \frac{\exp\{-U_3(s') + 2 \ln [|\det \mathbf{M}_3(s', L_t \alpha_t)|]\}}{\exp\{-U_3(s) + 2 \ln [|\det \mathbf{M}_3(s, L_t \alpha_t)|]\}}. \quad (68)$$

For all cases $j = 1, 2, 3, 4$ the observable we calculate for each configuration is

$$O_j(s, L_t \alpha_t) = \frac{[\det \mathbf{M}_j(s, (L_t - 1) \alpha_t)]^2}{[\det \mathbf{M}_j(s, L_t \alpha_t)]^2}. \quad (69)$$

By taking the ensemble average of $O_j(s, L_t \alpha_t)$ we obtain

$$\frac{Z_{N,N}(t - \alpha_t)}{Z_{N,N}(t)} \quad (70)$$

for $t = L_t \alpha_t$.

V. PRECISION TESTS AND PERFORMANCE COMPARISONS

A. Precision tests for two particles

We perform precision tests of the four auxiliary-field methods using the two-particle system at unitarity. For the system with one up spin and one down spin, we compute the dimensionless combination $mL^2 E_{1,1}(t)$ for $L = 4$ and $L_t = 6, 12$. As explained in the previous section we use hybrid Monte Carlo for $j = 1, 2, 4$ and the Metropolis algorithm for $j = 3$. The simulations are performed using 16 processors starting with different random number seeds producing independent configurations. The final result is computed from the average of the individual processor results, and the standard deviation is used to estimate the error of the average. The linear space of states for the two-particle system is small enough that the transfer matrix without auxiliary field in Eq. (22) can be used to calculate exact results for comparison. The results are shown in Table II. For each case, $j = 1, 2, 3, 4$, the auxiliary-field Monte Carlo results using M_j reproduce the exact results up to the estimated stochastic errors.

B. Performance comparisons

In our discussion $E_{N,N}^{0,\text{free}}$ refers to the ground state energy for N up-spin and N down-spin free fermions on the lattice. More explicitly $E_{N,N}^{0,\text{free}}$ is the energy exponent of the free-particle

TABLE II: Comparison of exact transfer matrix results and $j = 1, 2, 3, 4$ auxiliary-field Monte Carlo results for $mL^2 E_{1,1}(t)$ with $L = 4$ and $L_t = 6, 12$.

L_t	Exact result	M_1	M_2	M_3	M_4
6	-2.087	-2.06(3)	-2.10(3)	-2.05(4)	-2.10(3)
12	-2.817	-2.77(3)	-2.81(4)	-2.80(4)	-2.88(4)

transfer matrix,

$$: \exp(-H_{\text{free}}\alpha_t) : \left| \Psi_{N,N}^{0,\text{free}} \right\rangle = \exp\left(-E_{N,N}^{0,\text{free}}\alpha_t\right) \left| \Psi_{N,N}^{0,\text{free}} \right\rangle, \quad (71)$$

for the same lattice parameters used to calculate $E_{N,N}(t)$. In contrast with this lattice energy definition for $E_{N,N}^{0,\text{free}}$, we define the Fermi energy E_F purely in terms of particle density. For N up spins and N down spins in a periodic cube we let

$$E_F = \frac{k_F^2}{2m} = \frac{1}{2m} \left(6\pi^2 \frac{N}{L^3}\right)^{2/3} \simeq 7.596 \frac{N^{2/3}}{mL^2}. \quad (72)$$

For $N > 1$ it is useful to define the dimensionless function

$$\xi_{N,N}(t) = \frac{E_{N,N}(t)}{E_{N,N}^{0,\text{free}}}. \quad (73)$$

Scale invariance at unitarity requires that in the continuum limit $\xi_{N,N}(t)$ depends only on the dimensionless combination $\frac{t}{mL^2}$. For fixed N the Fermi energy E_F is proportional to $\frac{1}{mL^2}$, and so we can regard $\xi_{N,N}(t)$ as a universal function of $E_F t$. This universal behavior provides a simple but nontrivial check of scale invariance in our lattice calculations.

As one part of our analysis of computational performance we monitor the rejection rate at Step 6 of the hybrid Monte Carlo algorithm for $j = 1, 2, 4$ as well as the Metropolis update for $j = 3$. The average likelihood of rejection is recorded as a rejection probability P_r . Another aspect we monitor is the frequency of generating configurations with nearly singular matrices $\mathbf{M}_j(s, L_t\alpha_t)$. For this we introduce a small positive parameter δ and reject configurations with

$$|\det \mathbf{M}_j(s, L_t\alpha_t)| < \delta^N \left| \prod_{i=1,\dots,N} [\mathbf{M}_j(s, L_t\alpha_t)]_{ii} \right|. \quad (74)$$

By taking the limit $\delta \rightarrow 0^+$ we can determine if poorly-conditioned matrices make any detectable contribution to the final result. The rejection rate due to these singular matrices

is included in the total rejection probability P_r , but is also recorded separately as a singular matrix probability P_s .

We use double precision arithmetic in all calculations. Numerical stabilization methods based on Gram-Schmidt orthogonalization have been developed for determinantal quantum Monte Carlo simulations [55, 56, 57]. These methods have proved successful in reducing round-off error for singular matrix determinants and should also be effective here. However in our ground state lattice simulations we find that round-off error is only one of several problems associated with singular matrix configurations. Another problem that arises is quasi-non-ergodic behavior in the Monte Carlo updates. For the case of hybrid Monte Carlo importance sampling this problem can be visualized in terms of the landscape of the function $H_j(s, p)$ defined in Eq. (59). Each singular matrix configuration s produces a sharp peak in $H_j(s, p)$. Since hybrid Monte Carlo trajectories follow the contour lines of $H_j(s, p)$, these trajectories can get trapped on orbits around singular matrix configurations. Since the matrix inverse of \mathbf{M}_j diverges near these singular configurations, this behavior is also accompanied by large fluctuations in the difermion spatial correlation function

$$\left\langle a_{\downarrow}^{\dagger}(\vec{n})a_{\uparrow}^{\dagger}(\vec{n})a_{\uparrow}(0)a_{\downarrow}(0) \right\rangle. \quad (75)$$

This problem was observed in lattice simulations in [42]. For these reasons we take a cautious approach to singular matrix configurations until the problem is better understood. We use the singular matrix probability P_s as a diagnostic tool to measure the severity of the problem.

We use the unpolarized ten-particle system to test the computational performance of the four auxiliary-field methods. We compute $\xi_{5,5}(L_t\alpha_t)$ for spatial length $L = 5$ and temporal lengths $L_t = 24, 48, 72$. The simulations are performed using 8 processors starting with different random number seeds producing independent configurations. As before the individual processor results are averaged, and the standard deviation is used to estimate the error of the average. For $j = 1, 2, 4$ we generate hybrid Monte Carlo trajectories with $N_{\text{step}} = 10$ and $\varepsilon_{\text{step}} = 0.1$. For the $j = 3$ Metropolis update we flip the sign of s for 0.15% of lattice sites selected randomly on each lattice sweep. For the singular matrix condition in Eq. (74), we use $\delta = 5 \times 10^{-7}$.

Results for $\xi_{5,5}(L_t\alpha_t)$ for $L_t = 24$ are shown in Fig. 3. For $j = 1, 2, 4$ the horizontal axis is the number of completed hybrid Monte Carlo trajectories per processor. For $j = 3$

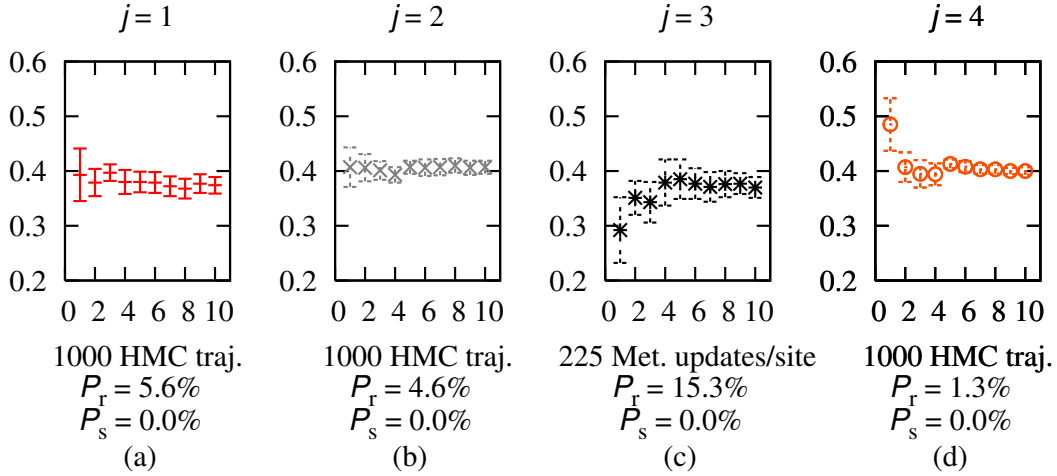


FIG. 3: (Color online) Monte Carlo results for $\xi_{5,5}(L_t\alpha_t)$ for $L = 5$ and $L_t = 24$. P_r is the rejection probability, and P_s is the singular matrix probability.

the horizontal axis is the number of attempted Metropolis updates per lattice site. On an Intel Xeon processor the CPU run time for 1000 hybrid Monte Carlo trajectories is roughly the same as 150,000 lattice sweeps with Metropolis updating on 0.15% of the sites. This corresponds with 225 updates per site.

All four calculations are in agreement with an average value $\xi_{5,5}(24\alpha_t) \approx 0.39$. In all cases the estimated errors are relatively small. In order of increasing error, the error bars for $j = 4$ is smallest, then $j = 2$, $j = 1$, and $j = 3$. This is the same ordering we get by sorting rejection probability P_r from lowest to highest. The singular matrix probability P_s is zero in all cases.

Results for $L_t = 48$ are shown in Fig. 4. This time all four calculations are in agreement with $\xi_{5,5}(48\alpha_t) \approx 0.29$. In all cases the estimated errors are still rather small, but upon closer inspection there are some early signs of trouble for $j = 3$ and $j = 2$. For $j = 3$ the rejection probability is quite large. This suggests difficulties in sampling the space of discrete auxiliary-field configurations. For $j = 2$ the singular matrix probability P_s is 1.9%. This is approaching the level where the contribution due to singular matrices may be detectable above the background of stochastic error.

Results for $L_t = 72$ are shown in Fig. 5. The simulation for $j = 2$ has failed due to the high singular matrix probability. The calculations for $j = 1, 3, 4$ are consistent with a value

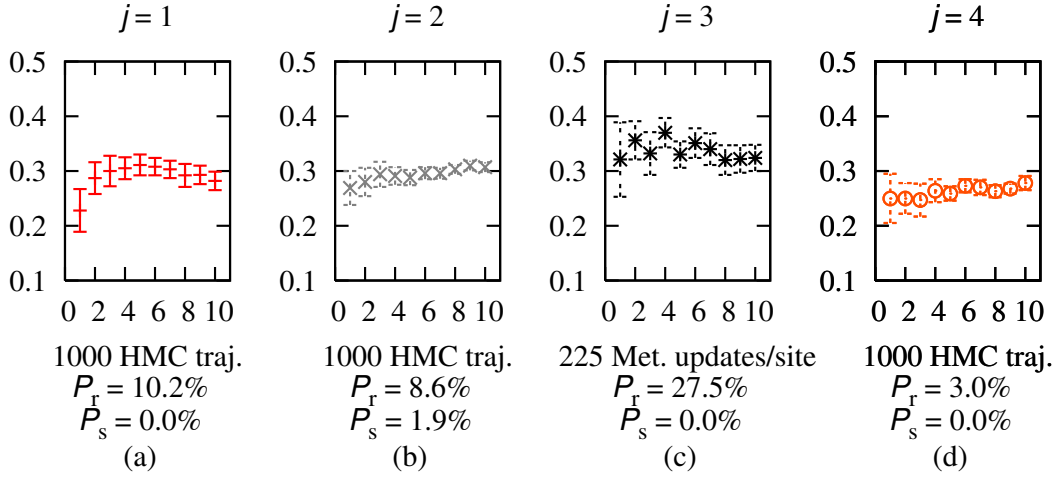


FIG. 4: (Color online) Monte Carlo results for $\xi_{5,5}(L_t\alpha_t)$ for $L = 5$ and $L_t = 48$.

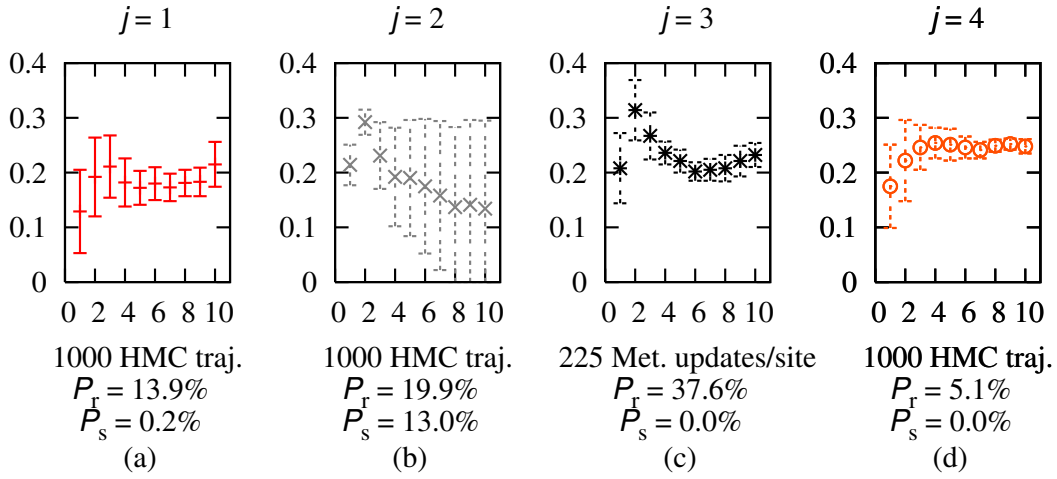


FIG. 5: (Color online) Monte Carlo results for $\xi_{5,5}(L_t\alpha_t)$ for $L = 5$ and $L_t = 72$.

of $\xi_{5,5}(72\alpha_t) \approx 0.25$. However the rejection probability for $j = 3$ is very high. This could explain the gradual downward and then upward drift in the $j = 3$ data, a sign that the Monte Carlo simulation has not fully equilibrated due to a long autocorrelation time. The same is true to a lesser extent for $j = 1$. For $j = 1$ we also see that P_s is small but nonzero. This suggests that problems with singular matrices may appear for somewhat larger L and L_t .

TABLE III: Lattice dimensions $L^3 \times L_t$ used in calculations for $\xi_{5,5}(L_t\alpha_t)$.

L^3	4^3	5^3	6^3	7^3	8^3
L_t	16	24	36	48	70
	20	30	42	56	80
	\vdots	\vdots	\vdots	\vdots	\vdots
	48	72	102	144	190

TABLE IV: Lattice dimensions $L^3 \times L_t$ used in calculations for $\xi_{7,7}(L_t\alpha_t)$.

L^3	4^3	5^3	6^3	7^3	8^3
L_t	12	18	30	40	50
	16	24	36	48	80
	\vdots	\vdots	\vdots	\vdots	\vdots
	44	72	96	128	170

From this analysis we rate the performance for $j = 4$ superior to the other three methods. This is not entirely unexpected. The use of a bounded auxiliary field should reduce the likelihood of exceptional configurations producing singular matrices. The use of a continuous auxiliary field makes it possible to use hybrid Monte Carlo which is better at reducing rejection probability than local Metropolis updates. For fixed trajectory length $N_{\text{step}}\varepsilon_{\text{step}}$, the rejection probability for hybrid Monte Carlo scales quadratically with step size, $\varepsilon_{\text{step}}^2$. This is in contrast with the Metropolis algorithm, where the rejection probability scales linearly with the fraction of lattice sites updated in each sweep. This contributes to a much slower performance of the Metropolis algorithm at large L and L_t .

VI. MAIN RESULTS

We use the bounded continuous auxiliary-field formulation $j = 4$ for the lattice results presented in this section. We consider the unpolarized ten-particle and the fourteen-particle systems. For the calculation of $\xi_{5,5}(L_t\alpha_t)$ we use the lattice dimensions $L^3 \times L_t$ shown in Table III. For $\xi_{7,7}(L_t\alpha_t)$ we use the lattice dimensions $L^3 \times L_t$ in Table IV. We use trajectory parameters $N_{\text{step}} = 10$, $\varepsilon_{\text{step}} = 0.1$, and singular matrix parameter $\delta = 5 \times 10^{-7}$.

The rejection probability P_r reaches a maximum of 12% and the singular matrix probability P_s reaches a maximum of 3% for the largest lattice volume, $L^3 = 8^3$ and $L_t \geq 170$. For most of the lattice simulations the values for P_r and P_s are much smaller. The simulations are run with a minimum of 16 processors each running a minimum of 10,000 hybrid Monte Carlo trajectories.

From Eq. (53) we expect

$$\xi_{N,N}(t) \approx \xi_{N,N} + \sum_{k \neq 0} \frac{|c_{N,N}^k|^2}{|c_{N,N}^0|^2} \left(\frac{E_{N,N}^k - E_{N,N}^0}{E_{N,N}^0} \right) e^{-(E_{N,N}^k - E_{N,N}^0)t} \quad (76)$$

at large t . To extract $\xi_{N,N}$ we perform a least squares fit of $\xi_{N,N}(t)$ to the functional form,

$$\xi_{N,N}(t) = \xi_{N,N} + b_{N,N} e^{-\delta_{N,N} E_F t}. \quad (77)$$

For asymptotically large $E_F t$, we can identify $\delta_{N,N} E_F$ with the energy separation between the ground state and the first excited state, possibly with degenerate partners. For large N the lowest excitation is expected to be a two phonon state with zero total momentum. For large N the excitation energy for this state is small compared with E_F and therefore $\delta_{N,N} \ll 1$.

Our observable $\xi_{N,N}(t)$ is proportional to the expectation value of the energy. When the energy difference $E_{N,N}^k - E_{N,N}^0$ is very small compared to $E_{N,N}^0$ the contribution proportional to $e^{-(E_{N,N}^k - E_{N,N}^0)t}$ is difficult to resolve against the background of stochastic noise. We note the factor

$$\frac{E_{N,N}^k - E_{N,N}^0}{E_{N,N}^0} \quad (78)$$

multiplying $e^{-(E_{N,N}^k - E_{N,N}^0)t}$ in Eq. (76). If the objective were to measure $E_{N,N}^k - E_{N,N}^0$ accurately for very low excitations, then it would be more effective to compute the Euclidean time projection of some other observable such as the difermion spatial correlation function

$$\left\langle a_{\downarrow}^{\dagger}(\vec{n}) a_{\uparrow}^{\dagger}(\vec{n}) a_{\uparrow}(0) a_{\downarrow}(0) \right\rangle. \quad (79)$$

This technique was used to identify the lowest energy excitations for several unpolarized lattice systems at unitarity [42].

In the analysis here we focus only on measuring the ground state energy accurately and ignore the numerically small contributions hidden in the asymptotic tail of $\xi_{N,N}(t)$. We

TABLE V: Results for the three-parameter fit for $\xi_{5,5}(t)$ using $b_{5,5}$, $\delta_{5,5}$, $\xi_{5,5}$.

L	$b_{5,5}$	$\delta_{5,5}$	$\xi_{5,5}$	$\chi^2/\text{d.f.}$
4	0.42(12)	0.47(13)	0.22(2)	1.2
5	0.40(7)	0.44(7)	0.23(1)	0.4
6	0.41(8)	0.42(8)	0.24(1)	1.6
7	0.81(18)	0.69(10)	0.26(1)	0.6
8	0.36(12)	0.32(15)	0.24(4)	0.6

TABLE VI: Results for the three-parameter fit for $\xi_{7,7}(t)$ using $b_{7,7}$, $\delta_{7,7}$, $\xi_{7,7}$.

L	$b_{7,7}$	$\delta_{7,7}$	$\xi_{7,7}$	$\chi^2/\text{d.f.}$
4	0.24(9)	0.39(13)	0.26(1)	1.3
5	0.28(4)	0.35(6)	0.27(1)	1.0
6	0.39(7)	0.45(6)	0.29(1)	1.3
7	0.29(8)	0.27(15)	0.26(4)	1.7
8	0.36(7)	0.41(10)	0.30(2)	0.8

determine $b_{N,N}$, $\delta_{N,N}$, $\xi_{N,N}$ from least squares fitting over the range $E_F t = 2$ to $E_F t = 9$. The values $b_{N,N}$ and $\delta_{N,N}$ we determine from least squares fitting should be interpreted as a spectral average,

$$\sum_{k \neq 0} \frac{|c_{N,N}^k|^2}{|c_{N,N}^0|^2} \left(\frac{E_{N,N}^k - E_{N,N}^0}{E_{N,N}^0} \right) e^{-(E_{N,N}^k - E_{N,N}^0)t} \approx b_{N,N} e^{-\delta_{N,N} E_F t}. \quad (80)$$

Since $\xi_{N,N}(t)$ has a well-defined continuum limit for fixed $E_F t$, each of the dimensionless parameters $b_{N,N}$, $\delta_{N,N}$, $\xi_{N,N}$ also has a well-defined continuum limit. Up to uncertainties the size of least squares fitting errors, $\xi_{N,N}$ is independent of the initial state overlap amplitudes $c_{N,N}^k$. However $b_{N,N}$ and $\delta_{N,N}$ both depend on $c_{N,N}^k$. Table V shows the three-parameter fit results for $N = 5$, and Table VI shows the three-parameter fit results for $N = 7$. The average chi-square per degree of freedom for the fits is about 1. The error estimates for the fit parameters are calculated by explicit simulation. We introduce Gaussian-random noise scaled by the error bars of each data point for $\xi_{N,N}(t)$. The fit is repeated many times with the random noise included to estimate the one standard-deviation spread in the fit parameters.

TABLE VII: Results for the two-parameter fit for $\xi_{5,5}(t)$ using $b_{5,5}, \xi_{5,5}$ with $\delta_{5,5} = 0.47$.

L	$b_{5,5}$	$\xi_{5,5}$	$\chi^2/\text{d.f.}$
4	0.42(4)	0.223(5)	1.0
5	0.43(4)	0.236(2)	0.3
6	0.47(3)	0.247(2)	1.5
7	0.51(4)	0.242(5)	0.9
8	0.47(4)	0.264(6)	0.6

TABLE VIII: Results for the two-parameter fit for $\xi_{7,7}(t)$ using $b_{7,7}, \xi_{7,7}$ with $\delta_{7,7} = 0.37$.

L	$b_{7,7}$	$\xi_{7,7}$	$\chi^2/\text{d.f.}$
4	0.23(2)	0.261(4)	1.1
5	0.29(1)	0.276(3)	0.9
6	0.31(2)	0.285(2)	1.4
7	0.34(4)	0.282(9)	1.6
8	0.33(3)	0.294(6)	0.8

The error in $\xi_{N,N}$ would be considerably smaller if the fit needed only two parameters rather than three parameters. This can be arranged if we neglect the L -dependence of $\delta_{N,N}$ and fix $\delta_{N,N}$ according to the average values for $L = 4, 5, 6, 7, 8$ as quoted in Tables V and VI. Since $\delta_{N,N}$ has a well-defined continuum limit, the L -dependence of $\delta_{N,N}$ should in fact be small. For $N = 5$ the average value is $\delta_{5,5} = 0.47$, and for $N = 7$ the average value is $\delta_{7,7} = 0.37$. Using these values we refit $\xi_{N,N}(t)$ with the two parameters $b_{N,N}, \xi_{N,N}$. Table VII shows the two-parameter fit results for $N = 5$, and Table VIII shows the two-parameter fit results for $N = 7$.

The average chi-square per degree of freedom is again about 1. The lattice data for $\xi_{5,5}(t)$ together with the two-parameter fit functions are shown Fig. 6. Fig. 7 shows the lattice data for $\xi_{7,7}(t)$ with two-parameter fit functions. The lattice results show that $\xi_{5,5}(t)$ and $\xi_{7,7}(t)$ are both approximately universal functions of $E_F t$ independent of L . This was expected from the scale invariance of the unitarity limit.

Using the results for $\xi_{5,5}$ and $\xi_{7,7}$ for $L = 4, 5, 6, 7, 8$ we can extrapolate to the continuum limit $L \rightarrow \infty$. We expect some residual dependence on L proportional to L^{-1} , arising from

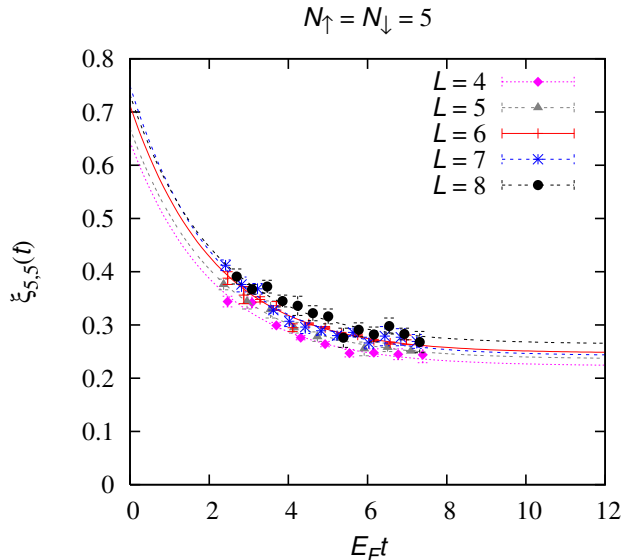


FIG. 6: (Color online) The lattice data for $\xi_{5,5}(t)$ versus $E_F t$ for $L = 4, 5, 6, 7, 8$. Also shown are the results of the two-parameter fits.

effects such as the effective range correction, broken Galilean invariance, and possibly other lattice cutoff effects. From the three-parameter fit results in Tables V and VI, the linear extrapolation in L^{-1} gives the continuum limit values

$$\xi_{5,5} = 0.308(25), \quad (81)$$

$$\xi_{7,7} = 0.337(30). \quad (82)$$

If we extrapolate the two-parameter fit results in Tables VII and VIII we get

$$\xi_{5,5} = 0.292(12), \quad (83)$$

$$\xi_{7,7} = 0.329(5). \quad (84)$$

Results from the two-parameter fits for $\xi_{5,5}$ and $\xi_{7,7}$ at finite L and the corresponding continuum limit extrapolations are shown in Fig. 8. We note that the continuum limit fit for $\xi_{N,N}$ could also be performed with $E_{N,N}^{0,\text{free}}$ defined in the continuum limit for the same cubic box size. This procedure is not recommended since it introduces a larger L^{-2} dependence and degrades the quality of the linear L^{-1} fit. However the fit can be done and the extrapolated values for $\xi_{5,5}$ and $\xi_{7,7}$ are each about 0.015 higher than the values reported in Eq. (83) and (84) with somewhat larger error bars.

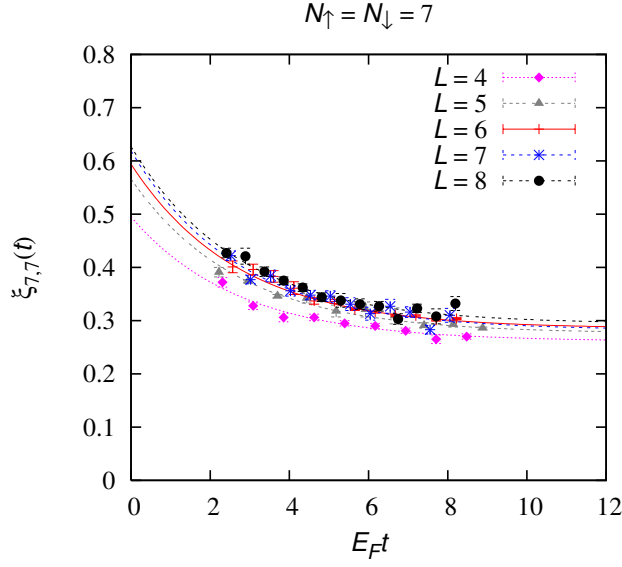


FIG. 7: (Color online) The lattice data for $\xi_{7,7}(t)$ versus $E_F t$ for $L = 4, 5, 6, 7, 8$. Also shown are the results of the two-parameter fits.

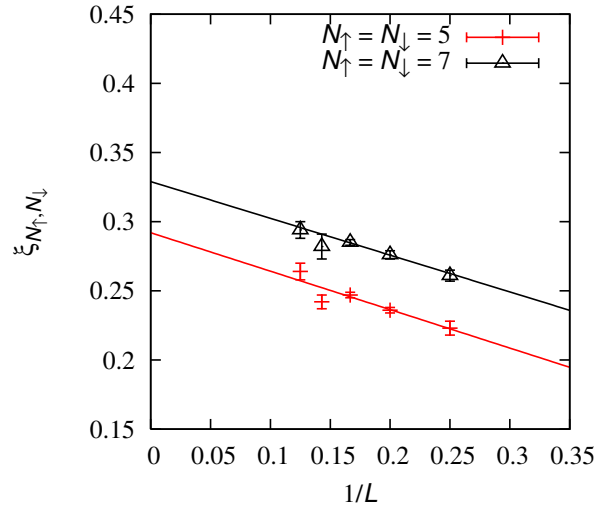


FIG. 8: (Color online) Results from the two-parameter fits for $\xi_{5,5}$ and $\xi_{7,7}$ at finite L and the corresponding continuum limit extrapolations.

VII. DISCUSSION

In [40] the values

$$\xi_{5,5} = 0.24(2), \quad (85)$$

$$\xi_{7,7} = 0.28(2), \tag{86}$$

were found based on an average of lattice results for $L = 4, 5, 6$. The results here for $\xi_{5,5}$ and $\xi_{7,7}$ with $L = 4, 5, 6$ are consistent with these values. The continuum limit extrapolation was not possible in [40] due to problems with increasing singular matrix probability P_s . That calculation used the auxiliary field formulation $j = 2$, which had the largest P_s of the four methods considered here. The bounded continuous auxiliary-field method appears to solve this problem for the lattice systems considered here. The values for $\xi_{5,5}$ and $\xi_{7,7}$ from small lattices $L = 4, 5, 6$ are each shifted upwards by 0.05 when extrapolated to the continuum limit.

In the calculations presented here we have only considered systems with 10 and 14 particles and have not attempted to determine the thermodynamical limit $N \rightarrow \infty$. It is therefore interesting to compare with results obtained using other methods that have computed ground state energies for both small and large values of N . Each of these other methods contain some unknown systematic errors, and so a benchmark comparison with continuum extrapolated Monte Carlo lattice results for $N = 5$ and $N = 7$ provides an estimate of the systematic error.

There is a discrepancy of about 0.13 in the reported values for $\xi_{5,5}$ and $\xi_{7,7}$ between continuum extrapolated lattice results and fixed-node Green's function Monte Carlo results on a periodic cube. The fixed-node Green's function Monte Carlo simulations find $\xi_{N,N} = 0.44(1)$ for $5 \leq N \leq 21$ [27] and 0.42(1) for larger N [28, 29]. This discrepancy suggests that the upper bound on the ground state energy using fixed-node Green's function Monte Carlo might be lowered further by a more optimal fermionic nodal surface.

A recent Hamiltonian lattice study computed $\xi_{N,N}$ for the range $N = 2$ to $N = 32$ on cubic lattices up to $L^3 = 16^3$ [41]. This calculation used a method called the symmetric heavy-light ansatz in the lowest filling approximation. In Fig. 9 we compare Monte Carlo lattice results presented here and symmetric heavy-light ansatz results for $N = 5$ and $N = 7$. The continuum limit extrapolations of the symmetric heavy-light results give

$$\xi_{5,5} = 0.301(1), \tag{87}$$

$$\xi_{7,7} = 0.339(1). \tag{88}$$

These results are within 0.01 of the values found in Eq. (83) and (84). This level of accuracy

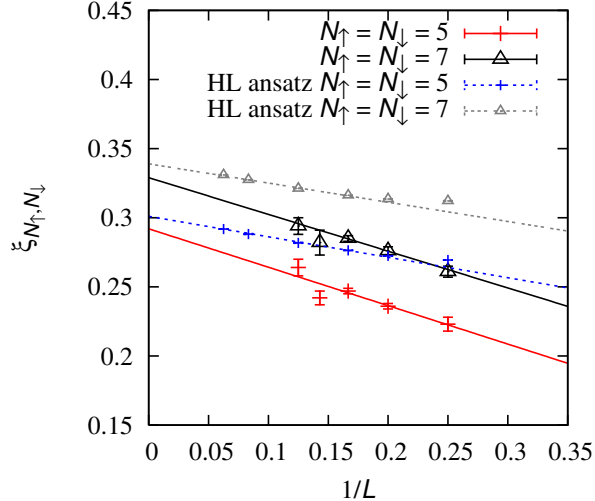


FIG. 9: (Color online) Comparison of results from Fig. 8 with Hamiltonian lattice results using the symmetric heavy-light ansatz in the lowest filling approximation.

is consistent with the size of errors found in [41] for four-body and six-body systems of the 1D, 2D, 3D attractive Hubbard models at arbitrary coupling.

The different L^{-1} slopes for the Hamiltonian lattice and Euclidean lattice extrapolations in Fig. 9 are consistent with the fact that the effective range for the Hamiltonian lattice interaction is a smaller negative fraction of the lattice spacing than for the Euclidean lattice transfer matrix. However there are other effects such as broken Galilean invariance on the lattice which produce a similar L^{-1} dependence [58]. An accurate calculation of the effective range correction with controlled systematic errors requires either an effective range larger than the lattice spacing or an analysis of the effect of changing the effective range parameter relative to the lattice spacing. The effective range correction has recently been computed on the lattice with realistic dilute neutron matter at next-to-leading order in chiral effective field theory [59, 60].

Results from the symmetric heavy-light ansatz for general N are shown in Fig. 10 [41]. We note that the value for $\xi_{N,N}$ reaches a maximum at $N = 7$. This can be explained by the closed shell at $N = 7$ in the free fermion ground state and the absence of shell effects in the interacting system. The numerical agreement for the benchmark comparisons at $N = 5$ and $N = 7$ provides some confidence in the symmetric heavy-light ansatz value of $\xi = 0.31(1)$ for the unitarity limit in the continuum and thermodynamic limits [41].

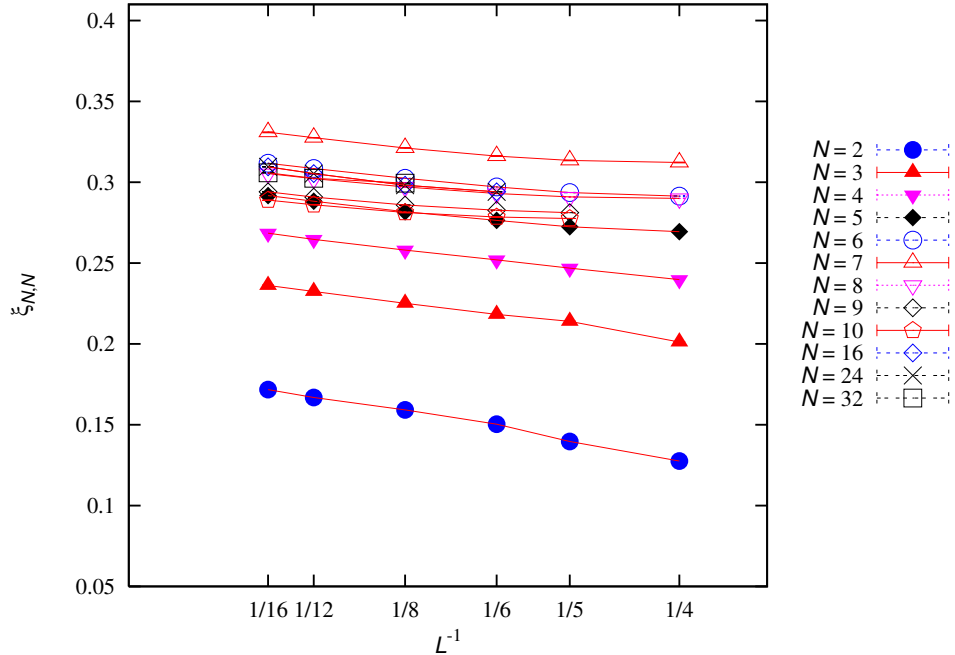


FIG. 10: (Color online) Results for $\xi_{N,N}$ at unitarity using the symmetric heavy-light ansatz in the lowest filling approximation [41].

The bounded continuous auxiliary-field method succeeds in reducing the singular matrix probability P_s by minimizing large fluctuations in the auxiliary-field transfer matrix elements. Very roughly this corresponds with reducing the size of

$$\max_{s(\vec{n}, n_t)} |A_j[s(\vec{n}, n_t)]|, \quad (89)$$

given the constraints

$$\int d_j s(\vec{n}, n_t) 1 = 1, \quad (90)$$

$$\int d_j s(\vec{n}, n_t) A_j[s(\vec{n}, n_t)] = 0, \quad (91)$$

$$\int d_j s(\vec{n}, n_t) A_j^2[s(\vec{n}, n_t)] = -C\alpha_t. \quad (92)$$

For lattice systems larger than the ones considered here the problem with singular matrices will reappear. For very large systems there may be no choice but to use the stabilization methods developed in [55, 56, 57] to reduce round-off error and confront the problems of large fluctuations and quasi-non-ergodic behavior using brute-force large-scale simulations. However for moderately larger systems it may be possible to gain further advantage using

a function $A_j[s(\vec{n}, n_t)]$ with a steep slope at $s(\vec{n}, n_t) = 0$ and relatively flat away from zero. The most extreme case would be to use an odd periodic step function. But this is equivalent to the discrete auxiliary-field formulation $j = 3$ with the problems discussed concerning large rejection probabilities. However with a smooth approximation to an odd periodic step function, it may be possible to reduce the singular matrix probability while at the same time compensate for the increase in rejection probability with a smaller hybrid Monte Carlo step size, $\varepsilon_{\text{step}}$.

VIII. SUMMARY

We have presented new Euclidean lattice methods which remove some computational barriers encountered in previous lattice calculations of the ground state energy in the unitarity limit. We compared the performance of four different auxiliary-field methods that produce exactly the same lattice transfer matrix. By far the best performance was obtained using a bounded continuous auxiliary field with hybrid Monte Carlo updating. With this method we calculated results for 10 and 14 fermions at lattice volumes $4^3, 5^3, 6^3, 7^3, 8^3$ and extrapolated to the continuum limit. For 10 fermions in a periodic cube, we found the ground state energy to be 0.292(12) times the ground state energy for non-interacting fermions. For 14 fermions the ratio is 0.329(5). These values may be useful as benchmarks for calculations of the unitarity limit ground state using other methods.

Acknowledgements

The author is grateful for discussions with Cliff Chafin, Gautam Rupak, and Thomas Schäfer. This work is supported in part by DOE grant DE-FG02-03ER41260.

-
- [1] D. M. Eagles, Phys. Rev. **186**, 456 (1969).
 - [2] A. J. Leggett, in *Modern Trends in the Theory of Condensed Matter. Proceedings of the XVIth Karpacz Winter School of Theoretical Physics, Karpacz, Poland, 1980* (Springer-Verlag, Berlin, 1980), p. 13.
 - [3] P. Nozieres and S. Schmitt-Rink, J. Low Temp. Phys. **59**, 195 (1985).

- [4] C. J. Pethick and D. G. Ravenhall, *Ann. Rev. Nucl. Part. Sci.* **45**, 429 (1995).
- [5] J. M. Lattimer and M. Prakash, *Science* **304**, 536 (2004), astro-ph/0405262.
- [6] K. M. O'Hara, S. L. Hemmer, M. E. Gehm, S. R. Granade, and J. E. Thomas, *Science* **298**, 2179 (2002).
- [7] S. Gupta, Z. Hadzibabic, M. W. Zwierlein, C. A. Stan, K. Dieckmann, C. H. Schunck, E. G. M. van Kempen, B. J. Verhaar, and W. Ketterle, *Science* **300**, 1723 (2003).
- [8] C. A. Regal and D. S. Jin, *Phys. Rev. Lett.* **90**, 230404 (2003).
- [9] T. Bourdel, J. Cubizolles, L. Khaykovich, K. M. F. Magalhaes, S. J. J. M. F. Kokkelmans, G. V. Shlyapnikov, and C. Salomon, *Phys. Rev. Lett.* **91**, 020402 (2003).
- [10] M. E. Gehm, S. L. Hemmer, S. R. Granade, K. M. O'Hara, and J. E. Thomas, *Phys. Rev.* **A68**, 011401(R) (2003).
- [11] M. Bartenstein, A. Altmeyer, S. Riedl, S. Jochim, C. Chin, J. Hecker Denschlag, and R. Grimm, *Phys. Rev. Lett.* **92**, 120401 (2004).
- [12] J. Kinast, A. Turlapov, J. E. Thomas, Q. Chen, J. Stajic, and K. Levin, *Science* **307**, 1296 (2005), cond-mat/0502087.
- [13] J. T. Stewart, J. P. Gaebler, C. A. Regal, and D. S. Jin, *Phys. Rev. Lett.* **97**, 220406 (2006), cond-mat/0607776.
- [14] J. R. Engelbrecht, M. Randeria, and C. S. de Melo, *Phys. Rev.* **B55**, 15153 (1997).
- [15] G. A. Baker, *Phys. Rev.* **C60**, 054311 (1999).
- [16] H. Heiselberg, *Phys. Rev.* **A63**, 043606 (2001), cond-mat/0002056.
- [17] A. Perali, P. Pieri, and G. C. Strinati, *Phys. Rev. Lett.* **93**, 100404 (2004).
- [18] T. Schäfer, C.-W. Kao, and S. R. Cotanch, *Nucl. Phys.* **A762**, 82 (2005), nucl-th/0504088.
- [19] T. Papenbrock, *Phys. Rev.* **A72**, 041603 (2005), cond-mat/0507183.
- [20] Y. Nishida and D. T. Son, *Phys. Rev. Lett.* **97**, 050403 (2006), cond-mat/0604500.
- [21] Y. Nishida and D. T. Son, *Phys. Rev.* **A75**, 063617 (2007), cond-mat/0607835.
- [22] J. Chen, *Chinese Phys. Lett.* **24**, 1825 (2007), nucl-th/0602065.
- [23] B. Krippa (2007), arXiv:0704.3984 [cond-mat.supr-con].
- [24] P. Arnold, J. E. Drut, and D. T. Son, *Phys. Rev.* **A75**, 043605 (2007), cond-mat/0608477.
- [25] P. Nikolic and S. Sachdev, *Phys. Rev.* **A75**, 033608 (2007), cond-mat/0609106.
- [26] M. Y. Veillette, D. E. Sheehy, and L. Radzihovsky, *Phys. Rev.* **A75**, 043614 (2007), cond-mat/0610798.

- [27] J. Carlson, S. Y. Chang, V. R. Pandharipande, and K. Schmidt, Phys. Rev. Lett. **91**, 50401 (2003), physics/0303094.
- [28] G. E. Astrakharchik, J. Boronat, J. Casulleras, and S. Giorgini, Phys. Rev. Lett. **93**, 200404 (2004), cond-mat/0406113.
- [29] J. Carlson and S. Reddy, Phys. Rev. Lett. **95**, 060401 (2005), cond-mat/0503256.
- [30] V. K. Akkineni, D. M. Ceperley, and N. Trivedi (2006), cond-mat/0608154.
- [31] O. Juillet, New Journal of Physics **9**, 163 (2007), cond-mat/0609063.
- [32] A. Bulgac, J. E. Drut, and P. Magierski, Phys. Rev. Lett. **96**, 090404 (2006), cond-mat/0505374.
- [33] A. Bulgac, J. E. Drut, P. Magierski, and G. Wlazlowski (2008), arXiv:0801.1504 [cond-mat.stat-mech].
- [34] E. Burovski, N. Prokofev, B. Svistunov, and M. Troyer, Phys. Rev. Lett. **96**, 160402 (2006), cond-mat/0602224.
- [35] E. Burovski, N. Prokofev, B. Svistunov, and M. Troyer, New J. Phys. **8**, 153 (2006), cond-mat/0605350.
- [36] D. Lee and T. Schäfer, Phys. Rev. **C73**, 015201 (2006), nucl-th/0509017.
- [37] D. Lee and T. Schäfer, Phys. Rev. **C73**, 015202 (2006), nucl-th/0509018.
- [38] T. Abe and R. Seki (2007), arXiv:0708.2523 [nucl-th].
- [39] T. Abe and R. Seki (2007), arXiv:0708.2524 [nucl-th].
- [40] D. Lee, Phys. Rev. **B73**, 115112 (2006), cond-mat/0511332.
- [41] D. Lee, Eur. Phys. J. **A35**, 171 (2008), arXiv:0704.3439 [cond-mat.supr-con].
- [42] D. Lee, Phys. Rev. **B75**, 134502 (2007), cond-mat/0606706.
- [43] S. Duane, A. D. Kennedy, B. J. Pendleton, and D. Roweth, Phys. Lett. **B195**, 216 (1987).
- [44] M. Lüscher, Commun. Math. Phys. **105**, 153 (1986).
- [45] S. R. Beane, P. F. Bedaque, A. Parreno, and M. J. Savage, Phys. Lett. **B585**, 106 (2004), hep-lat/0312004.
- [46] R. Seki and U. van Kolck, Phys. Rev. **C73**, 044006 (2006), nucl-th/0509094.
- [47] B. Borasoy, E. Epelbaum, H. Krebs, D. Lee, and U.-G. Meißner, Eur. Phys. J. **A31**, 105 (2007), nucl-th/0611087.
- [48] D. Lee and T. Schäfer, Phys. Rev. **C72**, 024006 (2005), nucl-th/0412002.
- [49] M. Creutz, Phys. Rev. **D38**, 1228 (1988).

- [50] M. Creutz, *Found. Phys.* **30**, 487 (2000), hep-lat/9905024.
- [51] R. L. Stratonovich, *Soviet Phys. Doklady* **2**, 416 (1958).
- [52] J. Hubbard, *Phys. Rev. Lett.* **3**, 77 (1959).
- [53] J. E. Hirsch, *Phys. Rev.* **B28**, 4059 (1983).
- [54] D. Lee, *Phys. Rev.* **A73**, 063204 (2006), physics/0512085.
- [55] G. Sugiyama and S. E. Koonin, *Ann. Phys.* **168**, 1 (1986).
- [56] S. Sorella, S. Baroni, R. Car, and M. Parrinello, *Europhys. Lett.* **8**, 663 (1989).
- [57] S. R. White, D. J. Scalapino, R. L. Sugar, E. Y. Loh, J. E. Gubernatis, and R. T. Scalettar, *Phys. Rev. B* **40**, 506 (1989).
- [58] D. Lee and R. Thomson, *Phys. Rev.* **C75**, 064003 (2007), nucl-th/0701048.
- [59] B. Borasoy, E. Epelbaum, H. Krebs, D. Lee, and U.-G. Meißner, *Eur. Phys. J.* **A34**, 185 (2007), arXiv:0708.1780 [nucl-th].
- [60] B. Borasoy, E. Epelbaum, H. Krebs, D. Lee, and U.-G. Meissner, *Eur. Phys. J.* **A35**, 357 (2008), arXiv:0712.2993 [nucl-th].